Solid State Sciences 20 (2013) 127–134

Contents lists available at SciVerse ScienceDirect

Solid State Sciences

journal homepage: www.elsevier.com/locate/ssscie

Electronic and optical properties of $ZnSc_2S_4$ and $CdSc_2S_4$ cubic spinels by the modified Becke–Johnson density functional

A. Bouhemadou [a,*], S. Al-Essa [b], D. Allali [a], M.A. Ghebouli [c], S. Bin-Omran [b]

[a] Laboratory for Developing New Materials and their Characterization, Department of Physics, Faculty of Science, University of Setif, 19000 Setif, Algeria
[b] Department of Physics and Astronomy, College of Science, King Saud University, P.O. Box 2455, Riyadh 11451, Saudi Arabia
[c] Department of Physics, University of Bordj Bou-Arreridj, 34000, Algeria

ARTICLE INFO

Article history:
Received 10 November 2012
Received in revised form
9 March 2013
Accepted 19 March 2013
Available online 28 March 2013

Keywords:
Cubic spinel sulfides
Ab initio calculations
Electronic properties
Optical properties

ABSTRACT

Structural, electronic and optical properties of the $ZnSc_2S_4$ and $CdSc_2S_4$ cubic spinels have been investigated by means of the full-potential (linearized) augmented plane wave plus local orbitals based on density functional theory. The exchange-correlation potential is treated by the GGA–PBEsol [J.P. Perdew, A. Ruzsinszky, G.I. Csonka, O.A. Vydrov, G.E. Scuseria, L.A. Constantin, X. Zhou, K. Burke, Phys. Rev. Lett. 100 (2008) 136406] and the recently proposed modified Becke–Johnson potential approximation (mBJ) [F. Tran, P. Blaha, Phys. Rev. Lett. 102 (2009) 226401], which successfully corrects the band-gap problem found with GGA for a wide range of materials. The obtained structural parameters are in good agreement with the available experimental data. This gives support for the predict properties for $ZnSc_2S_4$ and $CdSc_2S_4$. The band structures reveal that both compounds are semiconductor with a direct gap. The obtained gap values show that mBJ is superior for estimating band gap energy. We have calculated the electron and hole effective masses in different directions. The density of states has been analyzed. Based on our electronic structure obtained using the mBJ method we have calculated various optical properties, including the complex dielectric function $\varepsilon(\omega)$, complex index of refraction $n(\omega)$, reflectivity coefficient $R(\omega)$, absorption coefficient $\alpha(\omega)$ and electron energy-loss function $L(\omega)$ as functions of the photon energy. We find that the values of zero-frequency limit $\varepsilon_1(0)$ increase with decreasing the energy band gap in agreement with the Penn model. The origin of the peaks and structures in the optical spectra is determined in terms of the calculated energy band structures.

1. Introduction

The spinel structure is named after the class of mineral spinel known as $MgAl_2O_4$ [1]. More generally, the spinel structure refers to the family of materials with chemical formula AB_2C_4, where A and B are either divalent (A = Mg, Zn, Cd…) and trivalent (B = B, Al, Ga, In…) or tetravalent (A = Si, Ge, Sn…) and divalent cations (B = Mg, Zn, Cd…) [2]. C usually stands for oxygen or one chalcogen [3]. These materials exhibit many different and interesting optical, electronic, elastic, thermodynamic and magnetic properties which make them candidate materials for numerous applications in geophysics, magnetism, catalysis and environment [4–9].

$ZnSc_2S_4$ and $ZnSc_2S_4$ materials belong to the spinel family [10–12]. Theoretical and experimental information on these two compounds are scarce. Yim et al. [10] reported some information on the structural (lattice parameter) and electrical properties of these compounds. Reil and his co-workers [11] reported some information about the structural properties of $CdSc_2S_4$. According to previously cited references, $ZnSc_2S_4$ and $ZnSc_2S_4$ have cubic symmetry, with space group 227 (*Fd3m*).

To the best of our knowledge, there are no previous detailed studies on the electronic and optical properties for the $ZnSc_2S_4$ and $ZnSc_2S_4$ materials except the band gap values at ambient temperature. So here we report some additional basic studies on these two less known materials. Ab initio calculations offer one of the most powerful tools for carrying out theoretical studies of an important number of physical and chemical properties of the condensed matter. We therefore think that it is worthwhile to perform an ab initio study on the structural, band structure, density of states, charge carrier effective mass, dielectric function, reflectivity coefficient, absorption coefficient, refractive index and electron energy-loss function for these two cubic spinel sulfides by using the full-potential (linearized) augmented plane wave plus local orbitals (FP-(L)APW + lo) method with the GGA–PBEsol method for the

* Corresponding author. Tel./fax: +213 36620136.
E-mail address: a_bouhemadou@yahoo.fr (A. Bouhemadou).

1293-2558/$ – see front matter © 2013 Elsevier Masson SAS. All rights reserved.
http://dx.doi.org/10.1016/j.solidstatesciences.2013.03.016

ground state properties and the modified Becke–Johnson (mBJ) approximation for the excited-state properties in order to provide some additional information to the existing data on the physical properties of these materials.

2. Calculation details

All physical properties of a material are related to its total energy. In the present work the electronic total energy calculations at 0 K were performed within the framework of the density functional theory (DFT) and an all electron method with the (linearized) augmented plane wave + local orbitals ((L)APW + lo) basis set as implemented in WIEN2k code [13]. In this method, the wave functions are expanded in a linear combination of radial functions time spherical harmonics inside non-overlapping muffin-tin spheres of radius R_{MT} surrounding each atom and in plane waves in the interstitial region between the spheres. The radii for the muffin-tin spheres were taken as large as possible without overlap between the spheres: $R_{MT}^{Zn} = 2.21$ atomic units(a.u.), $R_{MT}^{Cd} = 2.36$ a.u., $R_{MT}^{Sc}(ZnSc_2S_4) = 2.42$ a.u., $R_{MT}^{Sc}(CdSc_2S_4) = 2.34$ a.u., $R_{MT}^{S}(ZnSc_2S_4) = 1.96$ a.u. and $R_{MT}^{S}(CdSc_2S_4) = 2.1$ a.u. The maximum l for the expansion of the wave function in spherical harmonics inside the muffin tin spheres was taken to be $l_{max} = 10$. A plane wave cut-off $K_{max} = 4.0\,(a.u.)^{-1}$ is chosen for the expansion of the wave functions in the interstitial region. The k integrations over the Brillouin zone (BZ) are performed up to $10 \times 10 \times 10$ Monkorst–Pack mesh (MP) [14] (47 k-points in the irreducible Brillouin zone (IBZ)). The self-consistent calculations are considered to be converged when the total energy of the system is stable within 10^{-4} Ry. Atomic positions were relaxed until the forces were below0.5 mRy(a.u.)$^{-1}$. The exchange-correlation potential for structural properties was calculated using the generalized gradient approximation based on Perdew et al. (PBEsol) [15], while for electronic properties in addition to that, the modified Becke–Johnson (mBJ) potential approximation [16–18], which describes better many semiconductors and insulators, was applied. It is a well-known problem that the calculated band gap using DFT within the common LDA and GGA is most of the time severely underestimated. For example, the reported results of calculations on the electronic properties of some oxide and sulfide spinels have showed that the common LDA and GGA systematically underestimate the band gap value of the spinel compounds family [9,19–21]. This is due to the fact that DFT within the most popular approximations LDA and GGA is reliable theory for reproducing accurately the ground-state properties such as the structural properties but not for predicting the excited state properties such as band gap. At present some approximations beyond the LDA and GGA, such as GW, hybrid functional, LDA + U, LDA + DMFT…etc, are developed in order to describe accurately the electronic structure of semiconductors and insulators. However some of these methods are computationally expensive or not satisfactory in all cases [22]; for example the LDA + U method can only be applied to correlated and localized electrons. Fortunately, the recently proposed modified Becke–Johnson (mBJ) potential approximation [16–18] is an alternative way to have a band gap close to the experimental value but computationally cheaper than the other mentioned methods. For spinel semiconductors and isolators, the mBJ method has been demonstrated to obtain band gaps in good agreement with the more accurate results obtained using GW method [20]. Tran and Blaha [22] have demonstrated that the mBJ potential yields band gaps which are in good agreement with experiment, leading to typical errors of less than 10% for some semiconductors and insulators. The drawback of the mBJ potential is that it cannot be obtained as the derivative of an X-Energy functional E_x [22]. Therefore, this potential cannot be used to calculate properties that depend on energy such as structural properties. In the present study the results obtained using GGA–PBEsol are compared to that obtained using the mBJ approach in order to show the advantage of the mBJ for describing electronic structure of herein studied materials.

3. Results and discussion

3.1. Structural properties

The unit cell of the cubic spinel AB_2C_4 contains eight AB_2C_4 formula units. The atomic positions depend on the chosen unit cell origin. There are two choices for the unit cell origin: the $\bar{4}3m$ on an A-site or $\bar{3}m$ on an octahedral vacancy. For the origin$\bar{3}m$, the eight A cations are positioned at the Wyckoff positions 8a (0.125, 0.125, 0.125) site, the sixteen B cations at *16d* (0.5, 0.5, 0.5), while the 32 anions, which are adjusted by the so-called C position parameter u, are located at 32e (u, u, u). For an ideal spinel, the internal parameter u has the value of 0.25 for the origin $\bar{3}m$. In cubic spinel, u is often found to be higher than 0.25. The increase in the value of u is associated with moving the anion C in the ⟨111⟩ direction outward from the nearest A site. So the cubic spinel crystalline structure is characterized by two parameters not fixed by the symmetry: the lattice constant a and the internal parameter u.

The first step in any ab initio calculation is to find the optimized geometry of the crystalline structure. The equilibrium lattice parameters of a crystal are the lattice parameters that minimize the total energy. Fitting the Murnaghan's equation of state (EOS) [23] to the primitive cell total energy versus its volume (with relaxed atom positions) yields the equilibrium primitive cell volume V_0, the bulk modulus B_0 and the pressure derivative of the bulk modulus B'. The obtained values for these mentioned parameters for the equilibrium ground state of $ZnSc_2S_4$ and $CdSc_2S_4$ compounds are listed in Table 1 along with available experimental results for comparison. The calculated values using GGA–PBEsol are in good agreement with the measured ones [10,11]. When the obtained equilibrium lattice constant values are compared with the experimental ones, we find a 0.45% underestimation. We have also calculated the equilibrium ground state parameters using the GGA in the Perdew–Burke–Ernzerhof (GGA-PBE) version [24] and the obtained lattice constants were with an overestimation of 1.2%. Therefore, we have performed all present calculation with the GGA–PBEsol. GGA–PBEsol is a recent approximation which has been developed specifically to improve the description of exchange-correlation energy in solids, resulting in structures and energetic for densely packed solids and their surfaces which are closer to the experiment in most cases.

3.2. Electronic band structure

For better understanding of the electronic and optical properties of $ZnSc_2S_4$ and $CdSc_2S_4$ cubic spinel compounds, the investigation of the electronic band structures would be useful. Fig. 1 displays our calculated band structures $E(k)$ on a discrete k mesh following high-

Table 1
Ground-state parameters of the $ZnSc_2S_4$ and $CdSc_2S_4$ cubic spinels: a is the lattice constant, u is the internal parameter, B_0 is the bulk modulus and B' is the bulk modulus pressure derivative.

	$ZnSc_2S_4$		$CdSc_2S_4$	
	Present	Exp.	Present	Exp.
a (Å)	10.4131	10.484 [10]	10.6847	10.733 [10] 10.736(2) [11]
u	0.2544	–	0.2601(3)	0.2601(2)
B_0 (GPa)	82.3	–	77.22	
B'	4.17	–	4.24	

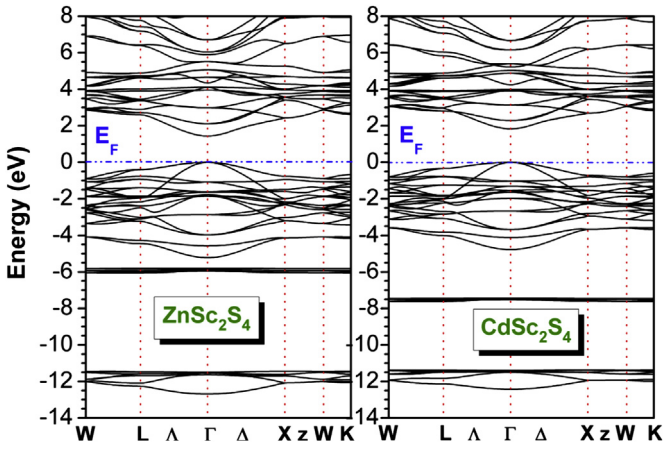

Fig. 1. Band structure for the most symmetrical directions in BZ, using the mBJ approximation for the $ZnSc_2S_4$ and $CdSc_2S_4$ compounds. The critical points that could compete for the definition of the gap are labeled. The horizontal dashed line indicates the position of the Fermi energy (E_F) which has been set equal to zero.

symmetry directions in the *k*-space at the equilibrium lattice parameters within the mBJ exchange-correlation potential for $ZnSc_2S_4$ and $CdSc_2S_4$. The calculated band structure profiles using the GGA–PBEsol and mBJ approximations for $ZnSc_2S_4$ ($CdSc_2S_4$) are similar except for the value of their band gaps which are higher within mBJ. For both compounds the valence band maximum (VBMa) and the conduction band minimum (CBMi) are located at Γ-point of the BZ, making them to be a direct band gap (Γ–Γ) materials. The obtained band gap values for the herein studied compounds using GGA–PBEsol and mBJ approximations are given in Table 2, along with the available experimental results [10] for comparison. From the results given in Table 2, it is clear that the obtained energy band gap using the mBJ approach is in better agreement with the experimental value than that obtained using the GGA–PBEsol for the two herein considered materials. The predicted band gap of $CdSc_2S_4$ using the mBJ (GGA–PBEsol) approach is 1.84 eV (0.79 eV) and is underestimated by about 20% (65%) compared to the only one reported experiment value of 2.3 eV. The predicted band gap of $ZnSc_2S_4$ using the mBJ (GGA–PBEsol) approach is 1.44 eV (0.39 eV) and is underestimated by about 30% (80%) compared to the only one reported experiment value of 2.1 eV. It is worth to note here that the experimental band gap values were extracted from the absorption coefficient versus wavelength spectra at room temperature and we don't have any idea about the incertitude of these measurements. We expect future experimental work to confirm out results. We can emphasize here that the mBJ approach improves significantly the band gap value of $ZnSc_2S_4$ and $CdSc_2S_4$ compared to the GGA–PBEsol, which is in agreement with recent reports about the advantages of the mBJ compared to the common LDA and GGA for a wide range of materials [20,22,25–31].

Table 2
Calculated band gap (E_g) at Γ and effective mass of the electron (m_e^*), the heavy hole (m_{hh}^*) and the light hole (m_{lh}^*) (in units of free electron mass m_0) using PBEsol and mBJ for the equilibrium ground-state of the cubic spinel $ZnSc_2S_4$ and $CdSc_2S_4$. The experimental energy band gaps are given for comparison.

	$ZnSc_2S_4$			$CdSc_2S_4$		
	PBEsol	mBJ	Expt.	PBEsol	mBJ	Expt.
E_g (eV)	0.39	1.44	2.1 [10]	0.79	1.84	2.3 [10]
$m_e^*(\Gamma\mapsto X)$	0.24	0.397		0.244	0.397	
$m_e^*(\Gamma\mapsto L)$	0.25	0.404		0.25	0.401	
$m_{hh}^*(\Gamma\mapsto X)$	0.63	0.82		0.70	0.91	
$m_{hh}^*(\Gamma\mapsto L)$	1.10	1.43		0.1.40	1.80	
$m_{lh}^*(\Gamma\mapsto X)$	0.23	0.35		0.23	0.35	
$m_{lh}^*(\Gamma\mapsto L)$	0.18	0.26		0.18	0.26	

The calculated total density of states (TDOS) and partial density of states (PDOS) for the $ZnSc_2S_4$ and $CdSc_2S_4$ cubic spinels in the energy range between −15 and 5 eV using the mBJ approach are illustrated in Fig. 2. The TDOS spectrum of $ZnSc_2S_4$ shows similar appearance as that of $ZnSc_2S_4$. Looking more closely to the DOS spectra of $ZnSc_2S_4$ and $ZnSc_2S_4$, four groups of valence bands, separated by direct gaps, can be visually identified. For $ZnSc_2S_4$ ($CdSc_2S_4$), the upper group of valence bands V1, occupies the energy range of 0 to −5.95 eV (0 to −4.10 eV). V1 is made up of 32 valence bands (24 valence bands). It is formed by the hybridization between S-3*p* states, Zn-3*d* (Cd-4*d*) and Sc-3*d* states, with a little contribution from Zn-3*p* (Cd-4*p*) and Sc-3*p* states. The second group V2, immediately below the upper group V1, is emanating from the hybridization between Zn-4*s* (Cd-5s), Sc-3*d* and S-3*p* states. The third one V3 is formed mainly from Zn-3*d* (Cd-4*d*) states, with a very small contribution from the Sc-3*d* and S-3*p* states. The lowest groupV4, not presented in Fig. 2 for more clarity of the DOS spectrum, which is centered at about −27.85 eV in both compounds, is composed of Sc-3*p* state contributions. The bottom of the conduction band C1 immediately above the Fermi level is mainly made up of Sc-3*d* states.

The effective charge-carrier mass is one of the main factors determining the transport properties, the Seebeck coefficient and electrical conductivity of materials. Here, the effective charge-carrier mass m^* has been evaluated by fitting the E–k diagram around the valence band maximum (VBMa) or the conduction band minimum (CBMi) by a paraboloid. The evaluated effective charge-carrier masses at the Γ point from the band dispersions of the VBMa and CBMi toward *X* and *L* directions in the Brillouin zone are summarized in Table 2 for the two materials under investigation (all in units of electron mass). The effective electron mass is indicated by the under script "e" (m_e^*), the heavy hole mass by "hh" (m_{hh}^*) and the light hole by "lh" (m_{lh}^*). Our calculations show that the charge-carrier effective masses have practically the same values in both materials, which predict that $ZnSc_2S_4$ and $CdSc_2S_4$ have practically same mobility of the charge-carrier. The electron effective mass values along the $\Gamma \to X$ and $\Gamma \to L$ directions in the BZ are practically equal, indicating its isotropy, and are close to that ones for typical semiconductor. The effective masses of holes are quite anisotropic.

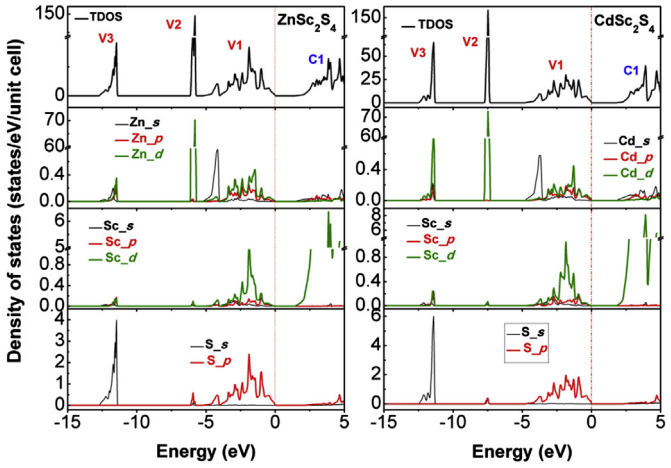

Fig. 2. Calculated total and partial densities of states (DOS and PDOS, respectively) by using mBJ approximation for the $ZnSc_2S_4$ and $CdSc_2S_4$ compounds. The vertical dashed line indicates the position of the Fermi energy (E_F) which has been set equal to zero.

3.3. Optical properties

Optical properties of a material are generally described by some physical parameters such as the dielectric function, absorption coefficient, refractive index, reflectivity coefficient, optical conductivity, and so on. All these optical parameters can be theoretically calculated from the frequency-dependent dielectric function $\varepsilon(\omega) = \varepsilon_1(\omega) + i\varepsilon_2(\omega)$ using the known formulas [32–34]. The dielectric function $\varepsilon(\omega)$ can be computed from knowledge of the electronic band structure of the considered material. The imaginary part $\varepsilon_2(\omega) = Im(\varepsilon(\omega))$ of dielectric function $\varepsilon(\omega)$ is calculated numerically by a direct evaluation of the matrix elements between the occupied and unoccupied electronic states [35]. The real part $\varepsilon_1(\omega) = \mathrm{Re}(\varepsilon(\omega))$ is calculated from $\varepsilon_2(\omega)$ using the Kramers–Krönig transform. It is worthwhile to note that in these calculations the local field effects are neglected. Phonon contributions to the optical spectra, which are especially important for the crystals with indirect band gap, are also not taken into account. However, even with these limitations the calculated spectra give reasonable agreement with experimental results [36].

Calculation of the optical properties requires a dense mesh of energy eigenvalues and the corresponding eigenvectors, so one needs to use finer meshes for the discretization of the BZ. Since $\varepsilon_2(\omega)$ is usually calculated first, we chose it as a reference for the assessment of convergence. The energy eigenvalues and eigenfunctions are then solved at 256 special k-points in the irreducible part of the BZ ($20 \times 20 \times 20$ k-point grids in BZ) for the optical properties.

Figs. 3 and 4 illustrate the computed imaginary part of the frequency-dependent dielectric function $\varepsilon_2(\omega)$ for the $ZnSc_2S_4$ and $CdSc_2S_4$ cubic spinels, respectively. The general patterns of $\varepsilon_2(\omega)$ curves of these two investigated compounds are rather similar. This similarity is attributed to the fact that the band structures of these compounds are similar with minor differences causing insignificant changes in the features of $\varepsilon_2(\omega)$. We note here that the increase of the band gap moving from $ZnSc_2S_4$ to $CdSc_2S_4$ causes the shift of the whole structures of $\varepsilon_2(\omega)$ spectrum to higher energy by 0.40 eV. There are no experimental or theoretical results on $\varepsilon_2(\omega)$ to compare with. The notable features of the $\varepsilon_2(\omega)$ spectrum were labeled (E_i) and quantitatively assessed in Tables 3 and 4.

We now address the origin of the transitions that are responsible for the spectral structures in the optical spectra. The determination

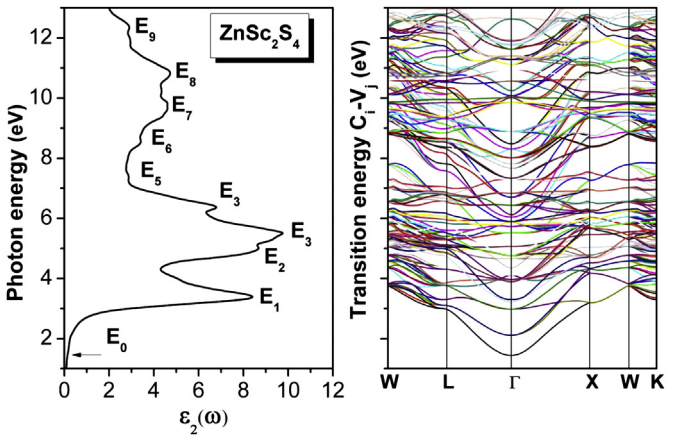

Fig. 3. Left-hand panel: contributions to the imaginary part of dielectric function $\varepsilon_2(\omega)$ from different band combinations. Right-hand panel: calculated transition band structure energy for the $ZnSc_2S_4$ compound. For the fine structure see Table 3. Conduction bands have been indexed starting from the lowest energy, while valence bands have indexed from the highest energy.

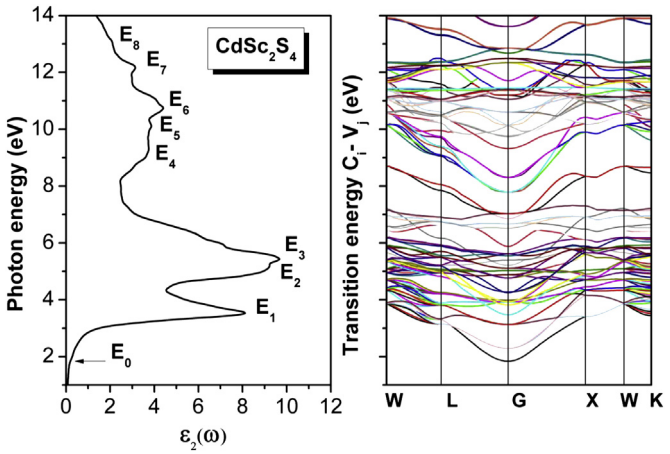

Fig. 4. Left-hand panel: contributions to $\varepsilon_2(\omega)$ from different band combinations. Right-hand panel: calculated transition band structure energy for the $CdSc_2S_4$ compound. For the fine structure see Table 4. Conduction bands have been indexed starting from the lowest energy, while valence bands have indexed from the highest energy.

of the origins of the different peaks and features of $\varepsilon_2(\omega)$ are performed on the basis of its decomposing to its individual pair contribution, i.e., contribution from each pair of valence v_i and conduction c_j bands ($v_i \rightarrow c_j$) (left-hand panels in Figs. 3 and 4), and plotting the transition (from valence to conduction) band structures, i.e., transition energy $E(k) = E_{cj}(k) - E_{vi}(k)$ (right-hand panels in Figs. 3 and 4). These techniques allow the knowledge of the bands which contribute more to the peaks and their locations in the Brillouin zone [37]. The main contributions to the optical spectra originate generally from the top valence bands to the lower conduction bands. The left-hand panel in Fig. 3 (4) represents the decomposition of $\varepsilon_2(\omega)$, performed for $ZnSc_2S_4$ ($CdSc_2S_4$), taking into consideration the fourteen top valence and the forty-two lowest conduction bands (thirty-one top valence and the thirty-eight lowest conduction bands) since these were the only ones found to contribute significantly to the dielectric function in the energy interval that include the transitions listed in Table 3 (4). The region, in which $\varepsilon_2(\omega)$ is different from zero, can be related to the absorption spectrum. The onset of the optical absorption edge in $\varepsilon_2(\omega)$, labeled E_0 in Figs. 3 and 4, occurs at approximately 1.44 eV and 1.84 eV in $ZnSc_2S_4$ and $CdSc_2S_4$, respectively. This corresponds to the direct optical band gap $\Gamma_v - \Gamma_c$, which gives the threshold for direct optical transition between the highest valence band and the lowest conduction band. This is known as the fundamental absorption edge. After that there is a sharp increase in the slope of $\varepsilon_2(\omega)$ and some structures centered at E_i points appear in $\varepsilon_2(\omega)$ spectrum. The positions of the main E_i peaks and the corresponding interband transitions and their locations in the Brillouin zone are reported in Tables 3 and 4.

The frequency-dependent real part of the dielectric function $\varepsilon_1(\omega)$ and frequency-dependent refractive index $n(\omega)$, which indicate how electromagnetic energy is dispersed when it penetrates in a material medium, are shown in Fig. 5 for the $ZnSc_2S_4$ and $CdSc_2S_4$ cubic spinels. The $\varepsilon_1(\omega)$ curve of $ZnSc_2S_4$ ($CdSc_2S_4$) presents two sharp peaks at 3.09 and 4.67 eV (3.29 and 4.70 eV) and two negative valleys, the first one is extended between 6.37 and 7.17 eV and the second one is between 10.75 and 19.05 eV (the first one is extended between 5.99 and 7.18 eV and the second one is between 10.83 and 18.37). As materials behave metallic for negative values of $\varepsilon_1(\omega)$ and are dielectric otherwise [38]. The static dielectric constant $\varepsilon_1(0)$ is given by the value of $\varepsilon_1(\omega)$ in the limit of zero energy limit (or infinite wavelength). Note that we do not include phonon contributions to the dielectric screening, and

Table 3
Peak positions (in eV) and the calculated origins of major contributions to structure in $\varepsilon_2(\omega)$ for $ZnSc_2S_4$. Conduction bands have been indexed starting from the lowest energy, while valence bands have been indexed from the highest energy.

Structure	Peak position (eV)	Major contribution transitions	Energy (eV)
E_1	3.39	(V_1–C_1) *W–L, X–W*	3.28
		(V_1–C_2) *W–L, X–W*	3.29
		(V_1–C_3) *W–L, Γ–X*	3.12, 3.46
		(V_1–C_4) *W–L–Γ–X*	3.19, 3.37
		(V_1–C_5) *W–L–Γ–X*	3.43, 3.71
		(V_1–C_6) *W–L, Γ–X*	3.41, 3.77
		(V_1–C_7) *W–L–Γ, X–W–K*	3.73, 4.35
		(V_1–C_8) *W–L, Γ–X–W–K*	4.02, 4.39
		(V_1–C_9) *W–L, Γ–X–W–K*	4.18, 4.52
		(V_1–C_{10}) *W–L, X–W*	4.53
		(V_1–C_{11}) *W–L–Γ–X, W–K*	4.16, 4.55
		(V_2–C_1) *W–L, X–W–K*	3.49
		(V_2–C_2) *W–L, X–W*	3.31
		(V_2–C_3) *W–L, Γ–X–W–K*	3.14, 3.84
		(V_2–C_4) *W–L–Γ–X*	3.20, 3.38
		(V_2–C_5) *L–Γ–X*	3.58
E_2	5.01	((V_1–C_{12}) *W–L, Γ–X, W–K*	4.54, 4.61, 4.70
		(V_1–C_{13}) *L–Γ–X*	4.64, 4.78
		(V_1–C_{14}) *W–L–Γ–X–W–K*	4.94
		(V_1–C_{15}) *L–Γ–X, W–K*	4.66, 5.00
		(V_1–C_{16}) *W–L–Γ–X–W–K*	5.05
		(V_1–C_{17}) *W–L, Γ–X*	5.14
		(V_1–C_{18}) *W–L, Γ–X, W–K*	5.37
		(V_1–C_{19}) *W–L–Γ*	5.29
		(V_2–C_9) *W–L, X–W–K*	4.74
		(V_2–C_{10}) *W–L, X–W*	4.74
		(V_2–C_{11}) *W–L, W–K*	4.83
		(V_2–C_{12}) *W–L, W–K*	4.83
		(V_2–C_{13}) *W–L*	5.10
		(V_2–C_{14}) *L–Γ–X–W*	4.83
		(V_2–C_{15}) *W–L–Γ–X*	5.03, 5.22
		(V_2–C_{16}) *W–L*	5.30
E_3	5.49	(V_2–C_{17}) *W–L, X–W–K*	5.54
		(V_2–C_{18}) *W–L, X–W–K*	5.54
		(V_2–C_{20}) *W–L–Γ*	5.46
		(V_{13}–C_4) *W–L, Γ–X–W–K*	5.30, 5.47
		(V_{13}–C_5) *L–Γ–X*	5.19
		(V_{13}–C_6) *W–L, Γ–X*	5.37
		(V_{13}–C_7) *W–L–Γ–X, W–K*	5.72
		(V_{13}–C_8) *W–L–Γ*	5.64
		(V_{13}–C_9) *W–L–Γ–X*	5.72
		(V_{13}–C_{10}) *W–L, Γ–X*	5.91
		(V_{13}–C_{11}) *W–L, Γ–X, W–K*	5.99
		(V_{13}–C_{12}) *W–L, Γ–X*	5.99
E_4	6.35	(V_1–C_{21}) *W–L–Γ–X*	6.78
		(V_1–C_{22}) *W–L–Γ–X*	6.84
		(V_1–C_{23}) *L–Γ–X*	6.80
		(V_2–C_{21}) *W–L, Γ–X–W–K*	6.79, 7.47
		(V_2–C_{22}) *W–L, Γ–X*	6.88
		(V_{13}–C_{13}) *W–L–Γ–X–W–K*	6.43
		(V_{13}–C_{14}) *W–L–Γ–X–W–K*	6.43
		(V_{13}–C_{15}) *L–Γ–X, W–K*	6.43
		(V_{13}–C_{16}) *Γ–X, W–K*	6.43
		(V_{13}–C_{17}) *W–L–Γ–X, W–K*	6.70
		(V_{13}–C_{18}) *W–L–Γ*	6.70
		(V_{13}–C_{19}) *W–L–Γ*	6.88
		(V_{13}–C_{20}) *W–L–Γ*	6.88
E_5	8.54	(V_1–C_{23}) *W–L, Γ–X, W–K*	8.64
		(V_1–C_{24}) *W–L, Γ–X–W–K*	8.02, 8.67, 8.85
		(V_1–C_{26}) *W–L–Γ–X, W–K*	8.13, 9.29
		(V_1–C_{27}) *W–L–Γ–X*	8.58
		(V_1–C_{28}) *W–L, Γ–X*	8.69, 8.93
		(V_1–C_{29}) *W–L–Γ–X*	8.05, 8.61
		(V_2–C_{23}) *W–L, X–W*	8.71
		(V_2–C_{24}) *W–L, X–W*	8.85
		(V_{13}–C_{21}) *W–L, Γ–X*	8.58
		(V_{13}–C_{22}) *W–L, Γ–X*	8.40
		(V_{14}–C_{27}) *L–Γ–X*	8.81
E_6	9.70	(V_{13}–C_{23}) *W–L–Γ–X*	9.03, 10.01
		(V_{13}–C_{24}) *W–L, Γ–X*	9.12, 9.54
		(V_{13}–C_{25}) *W–L, Γ–X*	9.40
		(V_{13}–C_{26}) *L–Γ–X*	9.40
		(V_{13}–C_{27}) *L–Γ–X*	9.93
		(V_{13}–C_{29}) *L–Γ*	9.83
		(V_{14}–C_{27}) *L–Γ–X*	9.91
E_7	10.19	(V_{13}–C_{24}) *W–L, Γ–X–W–K*	10.14
		(V_{13}–C_{28}) *W–L, Γ–X*	10.28
		(V_{13}–C_{30}) *W–L–Γ–X*	10.63
		(V_{13}–C_{31}) *W–L, Γ–X*	10.73
		(V_{14}–C_{27}) *W–L, Γ–X*	10.37
		(V_{14}–C_{28}) *W–L, Γ–X*	10.36
		(V_{14}–C_{29}) *L–Γ–X*	9.90, 10.32
		(V_{14}–C_{30}) *W–L–Γ–X*	10.73
E_8	10.81	(V_{13}–C_{32}) *W–L, Γ–X*	11.08
		(V_{13}–C_{33}) *W–L–Γ–X*	11.25
		(V_{13}–C_{34}) *L–Γ–X*	11.25
		(V_{13}–C_{35}) *W–L–Γ–X, W–K*	11.29, 11.51, 11.80
		(V_{14}–C_{31}) *W–L, Γ–X*	10.81
		(V_{14}–C_{32}) *W–L, Γ–X–W*	11.35
		(V_{14}–C_{33}) *L–Γ–X*	11.25
		(V_{14}–C_{34}) *L–Γ–X*	11.25
		(V_{14}–C_{35}) *L–Γ–X*	11.30, 11.62
E_9	12.34	(V_{13}–C_{36}) *L–Γ–X, W–K*	11.97
		(V_{13}–C_{37}) *W–L, Γ–X, W–K*	12.16
		(V_{13}–C_{38}) *W–L–Γ–X–W–K*	12.33
		(V_{13}–C_{39}) *L–Γ–X, W–K*	12.33
		(V_{13}–C_{40}) *L–Γ–X–W*	12.60
		(V_{13}–C_{41}) *W–L–Γ–X, W–K*	12.60
		(V_{13}–C_{42}) *W–L–Γ–X–W*	12.78
		(V_{14}–C_{35}) *L–Γ–X, W–K*	11.89
		(V_{14}–C_{36}) *W–L–Γ–X–W–K*	12.06
		(V_{14}–C_{37}) *W–L–Γ–X–W*	12.24
		(V_{14}–C_{38}) *W–L–Γ–X–W–K*	12.33
		(V_{14}–C_{39}) *W–L–Γ–X–W–K*	12.51, 12.06
		(V_{14}–C_{40}) *W–L–Γ–X–W–K*	12.68

$\varepsilon_1(0)$ corresponds to the static optical dielectric constant ε_∞. The calculated static dielectric constants $\varepsilon_1(0)$ values for $ZnSc_2S_4$ and $CdSc_2S_4$ are given in Table 2. We find that the values of $\varepsilon_1(0)$ decreases with increasing energy gap. This could be explained on the basis of the Penn model [39,40]. Penn model is based on the expression $\varepsilon_1(0) \approx 1 + (\hbar\omega_p/E_g)^2$. It is clear that $\varepsilon_1(0)$ is inversely proportional with E_g, hence smaller E_g yields larger $\varepsilon_1(0)$. We can determine E_g from this expression by using the value of $\varepsilon_1(0)$ and the plasma energy $\hbar\omega_p$.

The static refractive index $n(0)$ values and energy for which dispersion is null $E(n = 1)$ for $ZnSc_2S_4$ and $CdSc_2S_4$ are summarized in Table 5. In the far infrared region, the refractive index of $ZnSc_2S_4$ ($CdSc_2S_4$) is about 2.56 (2.49) and it increases with photon energy on the visible region reaching a peak in the ultraviolet at about 3.15 eV (3.32 eV). It then decreases to a minimum at 18.24 eV (17.15 eV). The origin of the structures in the imaginary part of the dielectric function also explains the structures in the refractive index. Unfortunately, no experimental values of these optical parameters were found in the literature, so these estimations remain to be purely theoretical. Knowledge of the refractive index is essential for devices such as photonic crystals, wave guides, solar cells, detectors and so on, therefore in addition to the mechanic quantum calculation, we have used some empirical models [41–43], relating the refractive index to the energy band gap, to estimate the static refractive index $n(0)$. The following models are used:

Table 4
Peak positions (eV) and the calculated origins of major contributions to structure in $\varepsilon_2(\omega)$ for $CdSc_2S_4$. Conduction bands have been indexed starting from the lowest energy, while valence bands have been indexed from the highest energy.

Structure	Peak position (eV)	Major contribution transitions	Energy (eV)
E_1	3.51	(V_1–C_1) *W–L–Γ–X–W*	2.24, 3.40
		(V_1–C_2) *W–L–Γ–X–W*	3.14, 3.46
		(V_1–C_3) *W–L, Γ–X*	3.51
		(V_1–C_4) *W–L, Γ–X*	3.33
		(V_1–C_5) *W–L–Γ–X*	3.76
		(V_1–C_6) *W–L–Γ–X*	3.47, 3.79
		(V_1–C_7) *W–L–Γ, X–W*	3.79, 4.34
		(V_1–C_8) *W–L–Γ–X–W*	3.93, 4.39
		(V_1–C_9) *W–L, Γ–X*	4.16
		(V_1–C_{10}) *W–L–Γ–X–W*	3.92, 4.48
		(V_1–C_{11}) *W–L–Γ–X–W*	4.02, 4.53
		(V_1–C_{12}) *W–L, Γ–X*	4.47
		(V_2–C_1) *W–L–Γ–X–W–K*	3.15, 3.61
E_2	5.24	(V_1–C_{13}) *L–Γ–X–W–K*	4.76
		(V_1–C_{14}) *L–Γ–X–W–K*	4.80
		(V_1–C_{15}) *W–L–Γ–X–W–K*	4.94
		(V_1–C_{16}) *L–Γ–X*	4.98
		(V_1–C_{17}) *W–L–Γ–X*	5.10
		(V_1–C_{18}) *W–L, Γ–X*	5.25
		(V_1–C_{19}) *W–L–Γ–X*	5.21
		(V_2–C_9) *W–L, X–W*	4.47
		(V_2–C_{10}) *W–L, X–W–K*	4.65
		(V_2–C_{11}) *W–L, Γ–X–W–K*	4.65
		(V_2–C_{12}) *W–L, X–W–K*	4.74
		(V_2–C_{13}) *W–L*	4.98
		(V_2–C_{14}) *W–L–Γ–X–W*	4.84, 5.06
		(V_2–C_{15}) *L–Γ–X*	4.92
		(V_{16}–C_1) *L–Γ–X*	4.65
		(V_{16}–C_2) *L–Γ–X–W*	4.93
E_3	5.45	(V_{14}–C_2) *W–L, Γ–X–W*	4.98, 5.22
		(V_{14}–C_3) *W–L, Γ–X*	5.27
		(V_{14}–C_4) *W–L, Γ–X*	5.27
		(V_{14}–C_5) *W–L–Γ–X–W–K*	5.27, 5.64
		(V_{14}–C_6) *W–L, Γ–X*	5.53
		(V_{14}–C_7) *W–L–Γ–X–W*	5.49, 5.77
		(V_{14}–C_8) *W–L, Γ–X–W*	5.81
		(V_{14}–C_9) *W–L, Γ–X–W*	5.91
		(V_{16}–C_4) *W–L–Γ–X*	5.37
		(V_{16}–C_5) *L–Γ–X*	5.54
E_4	9.24	(V_{13}–C_{23}) *W–L–Γ–X, W–K*	9.03, 9.77
		(V_{13}–C_{24}) *L–Γ–X*	8.93
		(V_{13}–C_{25}) *W–L–Γ–X*	8.53, 9.17, 9.49
		(V_{13}–C_{26}) *L–Γ–X*	9.45
		(V_{13}–C_{27}) *W–L–Γ–X*	9.92
		(V_{13}–C_{28}) *L–Γ–X*	8.40, 10.01
		(V_{13}–C_{29}) *W–L–Γ–X*	9.92, 10.63
		(V_{14}–C_{25}) *W–L–Γ–X–W*	8.85, 9.39, 10.36
		(V_{14}–C_{26}) *W–L, Γ–X*	9.83
E_5	10.15	(V_{13}–C_{30}) *W–L–Γ–X*	10.54, 10.81
		(V_{13}–C_{31}) *W–L, Γ–X*	10.81
		(V_{13}–C_{32}) *L–Γ–X*	10.46
		(V_{29}–C_1) *W–L–Γ, X–W*	10.32
		(V_{31}–C_1) *L–Γ–X*	10.00
E_6	10.73	(V_{13}–C_{32}) *W–L, Γ–X*	10.90
		(V_{13}–C_{33}) *W–L–Γ–X, W–K*	11.17
		(V_{13}–C_{34}) *L–Γ–X*	11.17
		(V_{13}–C_{35}) *W–L–Γ–X, W–K*	11.43, 11.61
		(V_{13}–C_{37}) *L–Γ–X*	11.43
		(V_{13}–C_{38}) *L–Γ–X*	11.44
		(V_{29}–C_2) *W–L, X–W–K*	10.54
		(V_{29}–C_3) *W–L, Γ–X–W–K*	10.63
		(V_{31}–C_1) *W–L, X–W–K*	10.36
		(V_{31}–C_2) *W–L, X–W–K*	10.50
		(V_{31}–C_3) *W–L, Γ–X–W–K*	10.63
		(V_{31}–C_4) *L–Γ–X–W–K*	10.73
E_7	12.14	(V_{13}–C_{36}) *W–L–Γ–X–W–K*	11.71
		(V_{13}–C_{37}) *L–Γ–X, W–K*	11.84
		(V_{13}–C_{38}) *L–Γ–X, W–K*	12.06
		(V_{29}–C_9) *W–L–Γ–X–W*	11.25
		(V_{29}–C_{10}) *W–L, Γ–X–W*	11.35
		(V_{29}–C_{11}) *L–Γ, X–W–K*	11.44
		(V_{29}–C_{13}) *W–L–Γ–X*	11.90
		(V_{29}–C_{14}) *L–Γ–X–W*	11.60, 12.12
		(V_{29}–C_{15}) *W–L, Γ–X*	12.06
		(V_{29}–C_{16}) *W–L, Γ–X*	12.16
		(V_{29}–C_{17}) *W–L, W–K*	12.16
		(V_{29}–C_{18}) *W–L, X–W*	12.24
		(V_{29}–C_{19}) *W–L–Γ–X*	12.33, 12.78
		(V_{31}–C_7) *W–L–Γ*	11.08
		(V_{31}–C_8) *W–L–Γ–X–W–K*	11.17
E_8	13.08	(V_{28}–C_{19}) *W–L–Γ–X*	12.33, 12.78
		(V_{28}–C_{20}) *W–L–Γ–X*	12.33, 12.78
		(V_{28}–C_{21}) *W–L, Γ–X–W*	12.78, 13.67
		(V_{28}–C_{22}) *W–L–Γ–X*	12.98, 13.54
		(V_{28}–C_{23}) *W–L, Γ–X*	14.65
		(V_{28}–C_{24}) *W–L–Γ–X–W*	14.56, 15.37
		(V_{29}–C_{20}) *L–Γ–X*	12.81
		(V_{29}–C_{21}) *W–L–Γ–X*	12.86, 13.67
		(V_{29}–C_{22}) *W–L, Γ–X*	13.58
		(V_{29}–C_{23}) *L–Γ–X*	13.99

(i) The Moss's formula [41] based on atomic model and given by:

$$E_g n^4 = k \tag{1}$$

E_g is the energy band gap and k is a constant with a value of 108 eV.

(ii) The Harve and Vandamme's empirical relation [42]:

$$n = \sqrt{1 + \left(\frac{A}{E_g + B}\right)^2} \tag{2}$$

with $A = 13.6$ eV and $B = 3.4$ eV.

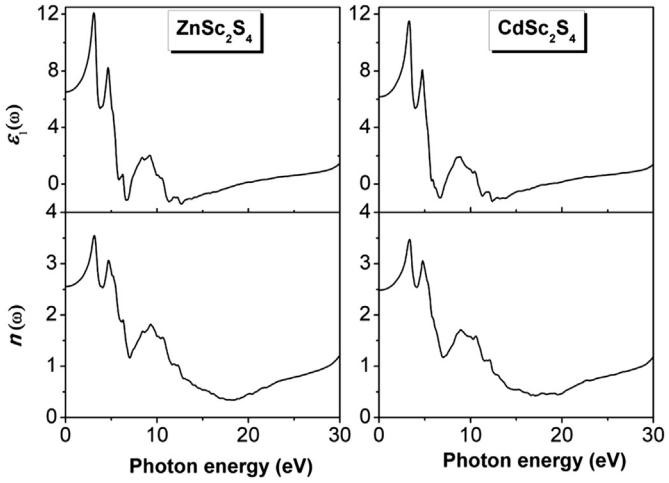

Fig. 5. Calculated real part of the frequency dependent dielectric function $\varepsilon_1(\omega)$ and refractive index $n(\omega)$ for the $ZnSc_2S_4$ and $CdSc_2S_4$ compounds.

Table 5
Characteristics values of the real part of the dielectric function ε_1 and the refractive index n. Energy is in eV, $\varepsilon_1(0)$ and $n(0)$ are adimensional.

	$ZnSc_2S_4$	$CdSc_2S_4$
ε(0)		
Ab initio	6.525	6.174
Model [32]	8.64	7.62
Model [33]	8.88	7.73
Model [34]	9.78	8.47
***n*(0)**		
Ab initio	2.5623	2.4858
Model [32]	2.94	2.76
Model [33]	2.98	2.78
Model [34]	3.13	2.91
$E(n=1)$	12.39	12.28
	28.64	28.92

(iii) The Ravindra and collaborators' relation [43]:

$$n = \alpha + \beta E_g,$$

where $\alpha = 4.048$ and $\beta = -0.62$ eV^{-1}.

The obtained values of the static refractive index for $ZnSc_2S_4$ and $CdSc_2S_4$ using previously mentioned empirical models with the calculated band gaps are summarized in Table 5. If we take in account that the calculated band gap could be slightly underestimated compared to the measured one, it appears that the refractive index values obtained using the empirical models are in agreement with the ones obtained using the ab initio calculations. Using the known relation $\varepsilon(0) = n^2$ we have also estimated $\varepsilon(0)$ via the previously mentioned models.

The numerically computed spectral dependence of the extinction coefficient $k(\omega)$, reflectivity coefficient $R(\omega)$ and absorption coefficient $\alpha(\omega)$, which represent different ways to describe how the electromagnetic energy is taken when interacting with a material medium, is depicted in Fig. 6.

The optical absorption coefficient $\alpha(\omega)$ is one of the most crucial evaluation criterions for the photoelectric materials. Our calculated absorption coefficient spectra $\alpha(\omega)$ for the herein investigated compounds show that these materials are a good optical absorption in a wide energy range (3–20 eV). These compounds can absorb in all frequency region which existed in ultraviolet light, so it can be used as a filter for various energies in the far UV spectrum. Fig. 6 shows similarities in the trends of extinction coefficient $k(\omega)$ and absorption coefficient.

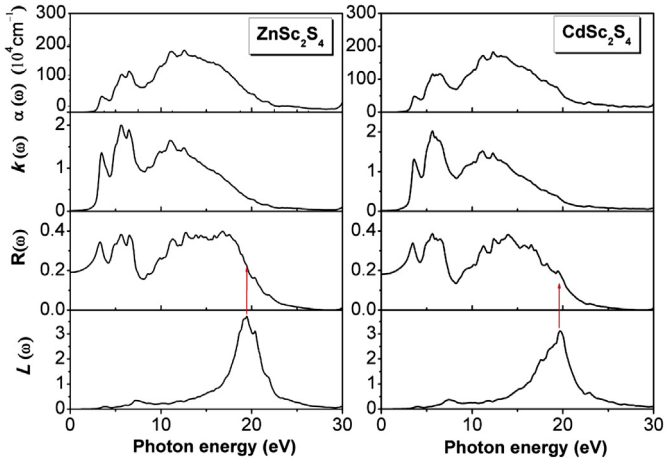

Fig. 6. Calculated absorption coefficient $\alpha(\omega)$, extinction coefficient $k(\omega)$, reflectivity coefficient $R(\omega)$ and electron energy-loss function $L(\omega)$ for the $ZnSc_2S_4$ and $CdSc_2S_4$ compounds.

The obtained $R(\omega)$ values for the therein studied materials do not approach to the unity toward zero energy ($R(0) = 19\%$), which means that these compounds behave like semiconductors. The computed reflectivity reaches a maximum value of around 40%. The reflectivity of both compounds is on the average between 16% and 40% up to 20 eV then beyond that it drops. The behavior of reflectivity makes these compounds particularly good for applications in visible and ultraviolet region.

Fig. 6 presents also the electron energy-loss function $L(\omega)$. $L(\omega)$ is an important factor describing the energy loss of a fast electron traversing the material. The peaks in $L(\omega)$ spectra represent the characteristic associated with the plasma resonance and the corresponding frequency is the so-called plasma frequency ω_p. The most remarkable descending branch in the reflectivity spectra coincides with a strong peak group in the energy-loss spectra as a result of the collective plasma resonance. The peaks of $L(\omega)$ correspond to the trailing edges in the reflection spectra, for instance, the maximum resonant electron-energy loss is at 19.48 eV for $ZnSc_2S_4$ and at 19.65 eV for $CdSc_2S_4$ corresponding to the abrupt reduction of $R(\omega)$.

4. Conclusions

In the present work, we have used an ab initio FP-L/APW + lo method to investigate the structural, electronic and optical properties of the $ZnSc_2S_4$ and $CdSc_2S_4$ cubic spinels. We have obtained very good agreement with the experimental lattice parameters by using GGA–PBEsol to the exchange-correlation energy. In order to provide a more accurate description of the electronic structure, we have also used the mBJ approximation to the exchange-correlation potential. We show that these two compounds are direct band gap semiconductors. Calculated energy band gap values by using the mBJ approach for the herein studied spinel sulfides are considerably improved and in better agreement with the experimental values compared to the GGA–PBEsol. The obtained DOS spectra are discussed. The effective charge-carrier masses are estimated from the band structure. We have investigated the photon-energy dependent dielectric function, refractive index, extinction coefficient, reflectivity coefficient, absorption coefficient and loss function. The decomposition of the dielectric functions into individual band-to-band contributions and the plotting of the transition band structures allowed identifying the microscopic origin of the features in the optical spectra and the contributions of the different regions in the Brillouin zone. We find that the values of $\varepsilon_1(0)$ increase with decreasing the energy gap. This could be explained on the basis of the Penn model. Our calculations of optical properties indicate that the herein studied materials could be candidates for applications in visible and ultraviolet region. As far as $ZnSc_2S_4$ and $CdSc_2S_4$ cubic spinels are concerned, some of our reported results are predictions and we welcome experiments to prove them.

Acknowledgments

This work was supported by the Deanship of Scientific Research at King Saud University for funding the work through the research group project No RGP-VPP-088.

References

[1] O.U. Okeke, J.E. Lowther, Phys. Rev. B 77 (2008) 094129.
[2] S.-H. Wei, S.B. Zhang, Phys. Rev. B 63 (2001) 045112.
[3] P. Garcia Casado, I. Rasines, J. Solid State Chem. 52 (1984) 187.

[4] A. Govindaraj, E. Flahaut, C. Laurent, A. Peigney, A. Rousset, C.N.R. Rao, J. Mater. Res. 14 (1999) 2567.
[5] G. Gusmano, G. Montesperelli, E. Traversa, G. Mattogno, J. Am. Ceram. Soc. 6 (1993) 743.
[6] N.J. Van der Laag, Environmental Effects on the Fracture of Oxide Ceramics. Doctorat Thesis, Technical University, Eindhoven, 2002.
[7] T. Irifune, K. Fujino, E. Ohtani, Nature 349 (1991) 409.
[8] R.J. Hill, J.R. Graig, G.V. Gibbs, Phys. Chem. Miner. 4 (1979) 317.
[9] S. Jiang, T. Lu, Y. Long, J. Chen, J. Appl. Phys. 111 (2012) 043516.
[10] W.M. Yim, A.K. Fan, E.J. Stolko, J. Electrochem. Soc. 120 (1973) 441.
[11] S. Reil, H.-J. Stork, H. Haeusler, J. Alloys Compd. 334 (2002) 92.
[12] R.E. Tressler, F.A. Hummel, V.S. Stubican, J. Am. Ceram. Soc. 51 (1968) 648.
[13] P. Blaha, K. Schwarz, G.K.H. Madsen, D. Kvasnicka, J. Luitz, WIEN2k: An Augmented Plane Wave + Local Orbitals Program for Calculating Crystal Properties, Karlheinz Schwarz, Techn. Universität, Wien, Austria, 2011. isbn:3-950131-1-2.
[14] H.J. Monkhorst, J.D. Pack, Phys. Rev. B 13 (1976) 5188.
[15] J.P. Perdew, A. Ruzsinszky, G.I. Csonka, O.A. Vydrov, G.E. Scuseria, L.A. Constantin, X. Zhou, K. Burke, Phys. Rev. Lett. 100 (2008) 136406.
[16] A.D. Becke, E.R. Johnson, J. Chem. Phys. 124 (2006) 221101.
[17] F. Tran, P. Blaha, Phys. Rev. Lett. 102 (2009) 226401.
[18] F. Tran, P. Blaha, K. Schwarz, J. Phys. Condens. Matter 19 (2007) 196208.
[19] S.Zh. Karazhanov, P. Ravindran, J. Am. Ceram. Soc. 93 (2010) 3335.
[20] H. Dixit, N. Tandon, S. Cottenier, R. Saniz, D. Lamoen, B. Partoens, V. Van Speybroeck, M. Waroquier, New J. Phys. 13 (2011) 063002.
[21] F. Semari, R. Khenata, M. Rabah, A. Bouhemadou, S. Bin Omran, A.H. Reshak, D. Rached, J. Solid State Chem. 183 (2010) 2818.
[22] D. Koller, F. Tran, P. Blaha, Phys. Rev. B 83 (2011) 195134.
[23] F. Murnaghan, Proc. Natl. Acad. Sci. U.S.A. 30 (1944) 244.
[24] J.P. Perdew, S. Burke, M. Ernzerhof, Phys. Rev. Lett. 77 (1996) 3865.
[25] A. Ghafari, A. Boochani, C. Janowitz, R. Manzke, Phys. Rev. B (2011) 125205.
[26] M.V. Lalić, Z.S. Popović, F.R. Vulkajlovi&cacute, Comput. Mat. Sci. 63 (2012) 163.
[27] San-Dong Guo, Bang-Gui Liu, J. Magn. Magn. Mater. 324 (2012) 2410.
[28] H.S. Saini, M. Singh, A.H. Reshak, M. Kashyak, J. Alloys Compd. 518 (2012) 74.
[29] J. Li, Z. Zhang, Q. Ji, H. Zhang, H. Luo, J. Alloys Compd. 537 (2012) 297.
[30] R. Ali, S. Mohammad, H. Ullah, S.A. Khan, U. Uddin, M. Khan, N.U. Khan, Physica B 410 (2013) 93.
[31] A.H. Reshak, S. Auluck, M. Piasecki, G.L. Myronchuk, O. Parasyuk, I.V. Kityk, H. Kamrudin, Spectrochim. Acta Part A 93 (2012) 274.
[32] L. Makinistian, E.A. Albanesi, Phys. Rev. B 74 (2006) 045206.
[33] C.M.I. Okoye, Eur. Phys. J. B 39 (2004) 5.
[34] C.M.I. Okoye, J. Phys. Condens. Matter 15 (2003) 5945.
[35] C. Amrosch-Draxl, J.O. Sofo, Comput. Phys. Commun. 175 (2006) 1.
[36] M.G. Brik, J. Phys. Chem. Solids 71 (2010) 1435.
[37] D. Allali, A. Bouhemadou, S. Bin-Omran, Comput. Mat. Sci. 51 (2012) 194.
[38] G. Murtaza, I. Ahmad, B. Amin, A. Afaq, M. Maqbool, J. Maqssod, I. Khan, M. Zahid, Opt. Mater. 33 (2011) 553.
[39] D.R. Penn, Phys. Rev. 128 (1960) 2093.
[40] A.H. Reshak, Z. Charifi, H. Baaziz, Eur. Phys. J. B 60 (2007) 463.
[41] V.P. Gupta, N.M. Ravindra, Phys. Status Solidi B 10 (1980) 715.
[42] J.P.L. Herve, L.K.J. Vandamme, Infrared Phys. Technol. 35 (1994) 609.
[43] N.M. Ravindra, S. Auluck, V.K. Srivastava, Phys. Status Solidi B 93 (1979) K155.